8-1-2023

On the Chemistry of Aqueous Ammonium Acetate Droplets During Native Electrospray Ionization Mass Spectrometry

Lars Konermann
konermann, konerman@uwo.ca

Zeyuan Liu

Yousef Haidar

Methew J. Willians

Nicholas A. Bainbridge

On the Chemistry of Aqueous Ammonium Acetate Droplets During Native Electrospray Ionization Mass Spectrometry

Lars Konermann*, Zeyuan Liu, Yousef Haidar, Mathew J. Willans, and Nicholas A. Bainbridge

Department of Chemistry, The University of Western Ontario, London, Ontario, N6A 5B7, Canada

* corresponding author: konerman@uwo.ca

Funding was provided by the Natural Sciences and Engineering Research Council of Canada (RGPIN-2018-04243).

ABSTRACT: Ammonium acetate (NH_4Ac) is a widely used solvent additive in native electrospray ionization (ESI) mass spectrometry. NH_4Ac can undergo proton transfer to form ammonia and acetic acid ($NH_4^+ + Ac^- \rightarrow NH_3 + HAc$). The volatility of these products ensures that electrosprayed ions are free of undesired adducts. NH_4Ac dissolution in water yields pH 7, providing "physiological" conditions. However, NH_4Ac is not a buffer at pH 7 because NH_4^+ and Ac^- are not a conjugate acid/base pair (L. Konermann, *J. Am. Soc. Mass Spectrom.* **2017**, *28*, 1827-1835). In native ESI it is desirable that analytes experience physiological conditions not only in bulk solution, but also while they reside in ESI droplets. Little is known about the internal milieu of NH_4Ac-containing ESI droplets. The current work explored the acid/base chemistry of such droplets, starting from pH 7 analyte solution. We used a two-pronged approach involving evaporation experiments on bulk solutions under ESI-mimicking conditions, as well as molecular dynamics simulations using a newly developed algorithm that allows for proton transfer. Our results reveal that during droplet formation at the tip of the Taylor cone, electrolytically generated protons get neutralized by Ac^-, making NH_4^+ the net charge carriers in the weakly acidic nascent droplets. During the subsequent evaporation, the droplets lose water as well as NH_3 and HAc that were generated by proton transfer. NH_3 departs more quickly because of its greater volatility, causing the accumulation of HAc. Together with residual Ac^-, these HAc molecules form an acetate buffer that stabilizes the average droplet pH at 5.4 ± 0.1, as governed by the Henderson-Hasselbalch equation. The remarkable success of native ESI investigations in the literature implies that this pH drop by ~1.6 units relative to the initially neutral analyte solution can be tolerated by most biomolecular analytes on the short time scale of the ESI process.

Introduction

Native electrospray ionization (ESI) mass spectrometry (MS) is widely used for the characterization of proteins and other biomolecular analytes.[1-12] During ESI, analyte solution is dispersed into charged droplets. These droplets undergo evaporation and jet fission,[13-15] culminating in progeny nanodroplets that release analyte ions into the gas phase.[13, 16] Native ESI relies on the fact that, under proper experimental conditions, gaseous biomolecular ions retain solution-like structures and interactions.[17-20] Mass analysis of these ions reveals their composition, while ion mobility spectrometry and other techniques provide additional insights.[1-12]

Most native proteins are stable in aqueous solution at near-neutral pH. Addition of acid or base may trigger unfolding and the loss of noncovalently bound ligands.[21] Buffers can ensure a suitable pH, both in living cells and in experiments.[22, 23] A typical solvent for traditional biochemical assays is 50 mM aqueous phosphate buffer, with 100 mM NaCl for additional ionic strength.[21] Unfortunately, such additives are unsuitable for ESI because they are nonvolatile, causing adducts, signal suppression, and chemical noise.[24, 25] Nonspecific adduction is consistent with the charged residue mechanism (CRM)[26] where ESI nanodroplets evaporate to dryness, causing analytes to associate with residual solutes in the vanishing droplet, thereby forming complexes that did not exist in bulk solution.[13, 16, 27] Sub-micrometer nanoESI tips can impart a higher salt tolerance,[28, 29] but this approach is not widely used.[30]

Most native ESI experiments employ aqueous solutions containing ammonium acetate (NH_4Ac).[1, 3, 19, 31-36] The popularity of this additive stems from two attributes: (1) NH_4Ac decomposes into NH_3 and acetic acid (HAc), both of which are volatile such that the resulting gaseous analyte ions are free of nonspecific adducts,[13] although some adduction can persist for certain systems.[37, 38] (2) NH_4Ac yields neutral pH when dissolved in water.[39] The second point has lead to the misconception that NH_4Ac is a neutral pH buffer.[39, 40] A buffer is defined as a "*solution*

containing appreciable amounts of both a weak acid and its conjugate weak base".[41] NH_4Ac is not a buffer at pH 7 because NH_4^+ and Ac^- are not a conjugate acid/base pair.[40] The conjugate acid of Ac^- is HAc, and the conjugate base of NH_4^+ is NH_3. Dissolution of NH_4Ac in water yields a neutral solution because $pK_a(HAc) = 4.76$ and $pK_a(NH_4^+) = 9.25$, such that $pH = 0.5 \times (4.76 + 9.25) = 7.01$.[42, 43] Although NH_4Ac is not a buffer at pH 7, it can still mitigate pH changes to some extent. Sub-stoichiometric addition of strong acid converts NH_4Ac to a Ac^-/HAc buffer. Analogously, sub-stoichiometric addition of strong base produces a NH_3/NH_4^+ buffer. The midpoints of these two buffers are defined by their pK_a values (4.76 and 9.25), and the range where they provide effective pH stabilization is $pK_a \pm 1$.[41] The buffering capacity of both systems in neutral solution is marginal, because both pK_a values are more than two units away from pH 7 (Figure 1).[13]

Inadvertent pH alterations during ESI can affect the outcome of experiments, e.g., by causing protein unfolding or the dissociation of complexes.[27, 44-54] We will focus on the commonly used positive ion mode, where water oxidation

$$2\ H_2O \rightarrow 4\ H^+ + O_2 + 4\ e^- \qquad (1)$$

is the main charge-balancing reaction, resulting in acidification of the solution in the emitter and in ESI droplets.[55] (We refer to protons in water as "H^+", although it would be more appropriate to describe them as H_3O^+, or $H_3O^+(H_2O)_n$.[56]) H^+ produced by eq. 1 are essential for imparting ESI droplets with their net charge, allowing for the production of gaseous $[M + zH]^{z+}$ analyte ions.[55] Even if the nascent droplets released from the Taylor cone are only mildly acidic, progressive solvent evaporation will continue to lower their pH,[57, 58] in extreme cases down to pH ≈ 1 or less.[40, 59, 60]

Techniques for interrogating ESI droplets include imaging,[61] phase-Doppler anemometry,[14] charge detection MS,[62, 63] and optical studies.[57, 58, 64-66] Unfortunately, the short lifetimes and size

heterogeneity of droplets in the ESI plume make it challenging to track their composition between production at the tip of the Taylor cone and evaporation to dryness.[13] Particular knowledge gaps persist for NH_4Ac-containing droplets. Water evaporation will tend to increase the NH_4Ac concentration, but ESI droplets may also experience loss of NH_4^+ and Ac^- (via evaporation of NH_3 and HAc, respectively). The implications of these processes for the internal droplet milieu are poorly understood. This lack of information is concerning, keeping in mind that nonnative environments can alter the properties of biomolecular analytes prior to their release into the gas phase.[27, 44-53]

The current work aims to uncover the properties of NH_4Ac-containing aqueous ESI droplets. Droplet fission is an important ESI component, but solvent evaporation represents an even more central element of the droplet evolution.[13] This is particularly evident for the CRM (which is believed to be prevalent during native ESI) where the final nanodroplets evaporate to dryness.[13, 16, 26] The importance of solvent evaporation is especially obvious for nanoESI, where nascent droplets released from the Taylor cone are very small, such that rapid evaporation with few fission events generates the final nanodroplets.[13, 28, 67] The idea behind the experiments performed here is that aspects of evaporating ESI droplets can be mimicked by tracking the evaporation of *bulk* NH_4Ac solutions, using strong acid (HCl) as surrogate for electrolytically generated protons (eq. 1). This approach allows the solution pH and composition to be measured during evaporation. Our experimental investigations were complemented by molecular dynamics (MD) simulations of ESI droplets, using a computational approach that for the first time considers the volatile nature of NH_4Ac. We find that initially neutral NH_4Ac analyte solutions undergo acidification to ~pH 5.4 during evaporation to dryness under native ESI conditions.

Experimental and Computational Methods

pH Calculations. The subsequent discussion requires a method for calculating the pH of an aqueous solution containing an amphiprotic salt, to which a strong acid has been added. We will specifically focus on NH_4Ac solutions after addition of HCl. Concentrations will be used instead of activities, which is an acceptable approximation for the solutions considered here.[43, 68] As outlined in the SI, the pH of a solution containing NH_4Ac and HCl can be calculated from eq. 2

$$[\mathrm{Cl^-}] + \frac{\mathrm{K_W}}{[\mathrm{H^+}]} + \frac{C_0\, K_\mathrm{W}}{[\mathrm{H^+}](K_\mathrm{b} + \frac{\mathrm{K_W}}{[\mathrm{H^+}]})} - \frac{[\mathrm{H^+}]C_0}{(K_\mathrm{a} + [\mathrm{H^+}])} - [\mathrm{H^+}] = 0 \qquad (2)$$

where C_0 is the initial NH_4Ac concentration, the added HCl concentration equals $[Cl^-]$ after equilibration, $K_a = K_a(NH_4^+) = 10^{-9.25}$, $K_b = K_b(Ac^-) = 10^{-9.24}$, and $K_w = 10^{-14}$. Eq. 2 can also be used for calculating pH after addition of strong base such as NaOH, by replacing $[Cl^-]$ with $(-1) \times [Na^+]$. A NH_4Ac titration curve calculated in this way is depicted in Figure 1 (solid symbols).

Eq. 2 reflects the behavior of the Ac^-/HAc and NH_3/NH_4^+ conjugate pairs across the entire pH range, but its application is cumbersome. By considering NH_4^+ and Ac^- as spectator ions at pH < 7 and pH > 7, respectively, the Henderson-Hasselbalch equation provides a simpler approach:

$$\mathrm{pH} = \mathrm{pK_a} + \log\frac{[\text{conjugate base}]}{[\text{conjugate acid}]} \qquad (3)$$

From eq. 3 it follows that the pH of a NH_4Ac solution with an initial pH of 7, after addition of HCl, can be calculated as

$$\mathrm{pH} = \mathrm{pK_a(HAc)} + \log\frac{[\mathrm{Ac^-}]_\mathrm{ini} - [\mathrm{Cl^-}]}{[\mathrm{HAc}]_\mathrm{ini} + [\mathrm{Cl^-}]} \qquad (4)$$

where $[HAc]_{ini} = C_0\,(10^{7-pKa} + 1)^{-1}$ and $[Ac^-]_{ini} = C_0 - [HAc]_{ini}$. Addition of NaOH can be treated analogously. The titration profile calculated using eq. 4 (Figure 1, solid line) is virtually identical to the results of eq. 2, justifying the use eqs 3 and 4 throughout the rest of this work.

Mass Spectrometry. Hen egg white lysozyme (14305 Da) and all other chemicals were from Sigma (St. Louis, MO). Native ESI mass spectra were acquired on a Synapt G2 mass spectrometer (Waters, Milford, MA) in positive ion mode using a Z-spray source at +2.8 kV and at a solution flow rate of 5 μL min^{-1}. All solutions were at pH 7, and the protein concentration was 5 μM. Conditions were adjusted to minimize collisional and thermal excitation of analyte ions (source temperature 30° C, desolvation temperature 40° C, sample cone 5 V, extraction cone 3 V, cone gas 50 L h^{-1}, desolvation gas 500 L h^{-1}, trap collision energy 4 V).

Evaporation Experiments. For tracking the evaporation of bulk solution samples, NH_4Ac was dissolved in water at 100 mM or 10 mM at pH 7. To model the effects of electrolytically generated protons in regular ESI (1500 nm initial droplet radius)[69] and nanoESI (150 nm initial droplet radius),[13] 2.69×10^{-5} M or 8.51×10^{-4} M HCl were added to these solutions, respectively. 25 mL samples were placed in beakers that were open to the atmosphere and kept at 70 to 85° C in a fume hood. Evaporation was stopped after various time periods by cooling the samples to room temperature. The extent of evaporation was then quantified by determining the relative solution volume (V_{REL}) gravimetrically; control experiments confirmed a constant solution density of (1.008 ± 0.004) g mL^{-1} in the [NH_4Ac] range of 10 mM to 1.0 M. V_{REL} = 1 corresponds to no evaporation, whereas 90% evaporation corresponds to V_{REL} = 0.1. Instead of removing aliquots from the solutions, every data point was based on an independent evaporation experiment starting with V_{REL} = 1. Evaporation to V_{REL} = 0.1 took ca. 1.5 h.

H-1 nuclear magnetic resonance (NMR) spectroscopy data were acquired at 25° C on a Bruker Neo 600 MHz spectrometer equipped with a 5 mm HX probe. Solution aliquots were spiked with 10% v/v D_2O for chemical shift locking, for a total sample volume of 400 μL. Combined [Ac^-] + [HAc] concentrations were measured by integrating the methyl peak, and by comparing the

measured peak areas with calibration profiles generated using [NH_4Ac] reference solutions. Calibrant plots were linear in the 10 mM to 1.0 M range with $R^2 > 0.99$. The methyl peak moved from 1.81 ppm at pH 7 to 1.99 ppm at pH 2.2, as a result of carboxylate protonation (Figure S1). An AB15 glass electrode pH-meter (Fisher Scientific, Mississauga, ON) was used for pH measurements. All experiments were conducted in triplicate with independent calibration profiles; error bars represent standard deviations.

Computational Methods. MD simulations were conducted using Gromacs 2020,[70] following established methods with some modifications.[16, 71, 72] Rayleigh-charged ESI droplets with an initial 3 nm radius were kept at 370 K for 50 ns, followed by 25 ns at 500 K. H-bonded ion pairs were given the opportunity to undergo $NH_4^+ + Ac^- \rightarrow NH_3 + HAc$ proton transfer in 250 ps intervals (Figure S2 and TOC Figure). All other details can be found in the SI.

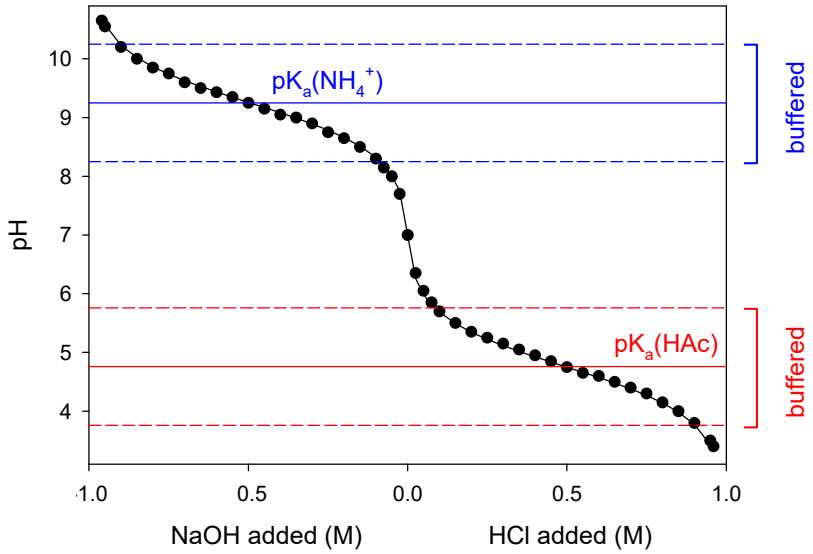

Figure 1. Calculated titration profile of aqueous NH_4Ac with an initial pH of 7 and $C_0 = 1$ M, upon addition of strong acid (HCl) or strong base (NaOH). Black circles represent data calculated using eq. 2. The solid line represents the Henderson-Hasselbalch approximation (eqs. 3 and 4). Dashed blue and red lines indicate the regions that match the definition of a buffer ($pH = pK_a \pm 1$).

Results and Discussion

Features of NH_4Ac Solutions. The volatile nature of NH_4Ac can be illustrated in simple experiments. A concentrated aqueous NH_4Ac solution was kept at 80° C in a beaker for 2 h, causing all of the water and 93% of the NH_4Ac to evaporate (Figure 2). The near-complete vaporization of NH_4Ac in Figure 2 is in striking contrast to solutions of nonvolatile salts such as NaCl, where all of the solute stays behind as solid residue after water evaporation.[73]

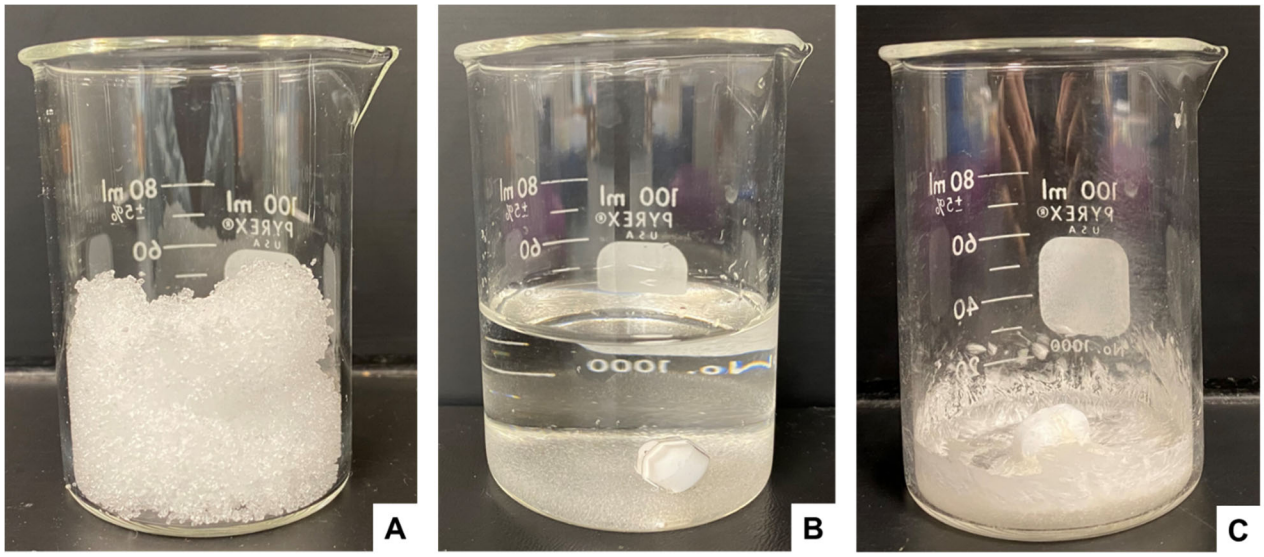

Figure 2. Demonstrating the volatile nature of NH_4Ac. (A) 22 g of NH_4Ac were placed in a beaker. (B) The salt was dissolved in 50 mL of H_2O/HAc at pH 5.5 (C_0 = 5.7 M). (C) After 2 h at 80° C, only 1.5 g of NH_4Ac remained as dry crystals. The beaker in panels B and C contains a stir bar.

Figure 3 compares the behavior of NaCl and NH_4Ac in native ESI-MS. Protein mass spectra generated with NaCl show extensive peak tailing due to the formation of heterogeneous $[M + zH + n(Na - H) + m(Cl + H)]^{z+}$ adducts, illustrated in Figure 3A for lysozyme. Figure 3A also shows abundant chemical noise in the form of salt clusters.[13, 24, 25] In contrast, ESI of lysozyme in 100 mM aqueous NH_4Ac yielded clean $[M + zH]^{z+}$ signals with greatly reduced background noise (Figure 3B), highlighting the favorable properties of this volatile salt.[1, 3, 19, 31-36]

Electrospraying aqueous solutions without analyte is instructive as well. NaCl solution generated a range of $Na_nCl_m^{(n-m)+}$ clusters (Figure 3C) resulting from association of Na^+ and Cl^- during the final stages of droplet evaporation, followed by CRM release into the gas phase.[72, 74, 75] This is in contrast to spectra obtained upon electrospraying aqueous NH_4Ac, where NH_4Ac cluster ions are unobservable (Figure 3D). The *m/z* 77 signal in Figure 3D corresponds to $[M + NH_4]^+$ of acetamide, which is a contaminant in commercially supplied NH_4Ac.[76]

Evaporation of ESI droplets in Figure 3D proceeds many orders of magnitude faster than under the bulk solution conditions of Figure 2, owing to the much larger surface-to-volume ratio of the droplets.[13] ESI-related events such as the formation of charged progeny droplets or the ejection of charge carriers (e.g., solvated NH_4^+) via the ion evaporation mechanism (IEM) cannot be expected for electrically neutral bulk solutions.[13, 16, 77] Nonetheless, the bulk evaporation of Figure 2 parallels the ESI droplet behavior in Figure 3. In both cases, most of the NH_4Ac enters the vapor phase as NH_3(g) and HAc(g) during evaporation of the solutions.[13] We therefore suggest that semi-quantitative insights into the behavior of evaporating NH_4Ac-containing ESI droplets can be obtained by examining the evaporation of bulk NH_4Ac solutions, an idea that will be explored in the subsequent sections.

Cornerstones of ESI Droplet Behavior. Prior to conducting bulk evaporation experiments, it is necessary to choose conditions that match the ESI droplet behavior as closely as possible. Figure 4 provides a simplified cartoon of events taking place in the ESI plume. Nascent droplets formed at the tip of the Taylor cone shrink to dryness as the result of evaporation and fission events.[61, 78] We will assume that solutes are uniformly distributed throughout the droplet (although this is not always the case, as discussed later). Analyte involvement in titration equilibria is not considered. In this scenario, the following conditions apply:

(i) Droplet Size. The radius r_0 of nascent droplets depends on the ESI regime.[79] Regular ESI, with emitter diameters of ca. 100 µm and flow rates in the µL min^{-1} range produces nascent droplets with $r_0 \approx 1500$ nm.[69] NanoESI emitters and flow rates are at least one order of magnitude smaller, resulting in $r_0 \approx 150$ nm.[13] We will make reference to these two regimes, when discussing nascent droplets in regular and nanoESI.

(ii) NH_4Ac Concentration. Typical native ESI experiments start with bulk solutions with an initial pH of 7, containing C_0 = 10 mM to 100 mM NH_4Ac.[1, 3, 19, 31-36] Thus, we will focus on these two C_0 values. Nascent droplets formed at the tip of the Taylor cone have not undergone extensive evaporation yet, such their NH_4Ac concentrations will be close to C_0, albeit with some $Ac^- \rightarrow HAc$ conversion, see point (*v*).

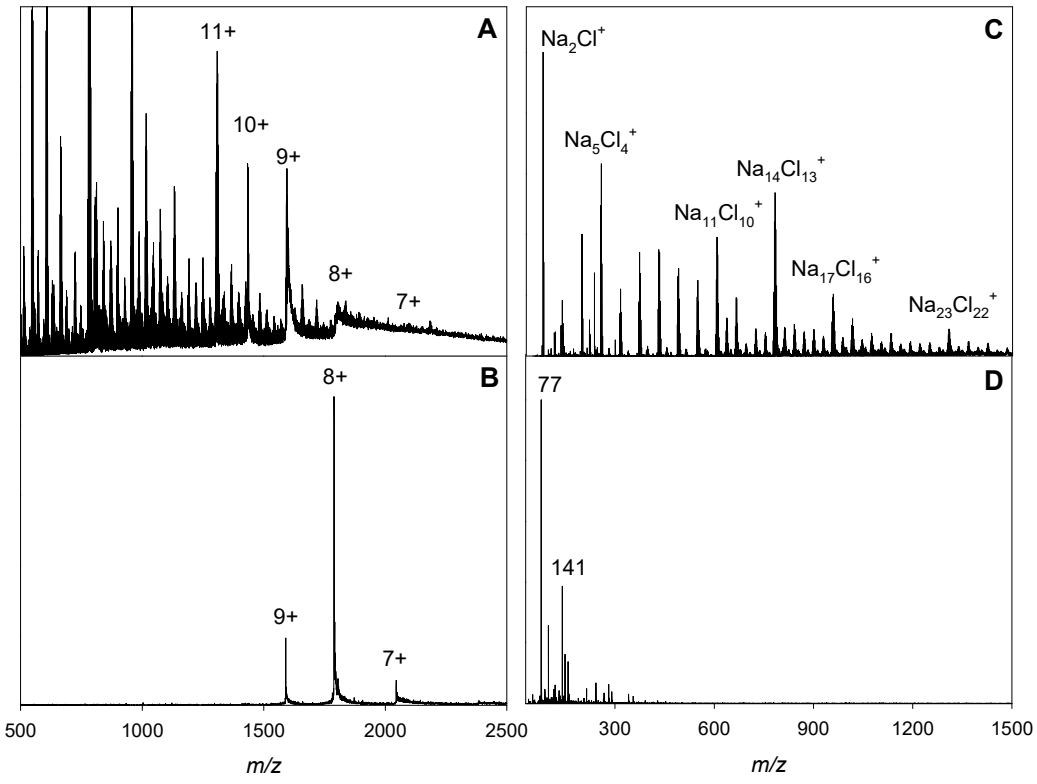

Figure 3. ESI mass spectra acquired for aqueous pH 7 solutions. (A) Lysozyme in 5 mM NaCl. (B) Lysozyme in 100 mM NH_4Ac. Charge states of protein ions are indicated as 7+, 8+, etc. (C) 10 mM NaCl. The composition of selected cluster ions is indicated. (D) 100 mM NH_4Ac. The samples used for panels C and D did not contain any analytes other than the dissolved salts.

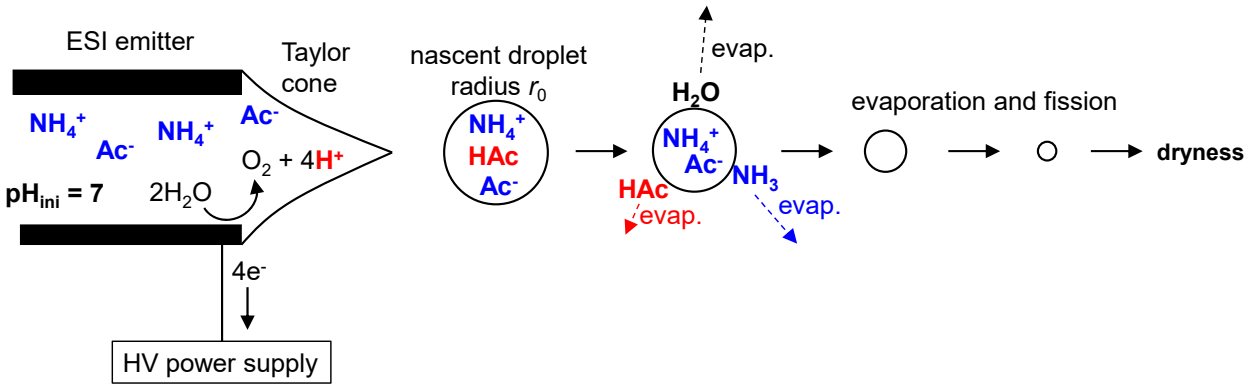

Figure 4. Simplified cartoon of native ESI with NH_4Ac solution. Components are not shown to scale. The analyte solution prior to ESI has pH 7. Droplets are acidified by H_2O electrolysis, converting some Ac^- to HAc. The droplets then undergo evaporation of water, NH_3, and HAc. Evaporation and fission events eventually cause droplet shrinkage to dryness.

(iii) Droplet Charge. Nascent droplets are close to the Rayleigh limit (Figure S3A), where the net number of charges is

$$z_R = 8\pi/e \times (\varepsilon_0 \gamma r^3)^{1/2} \qquad (5)$$

with the surface water tension $\gamma = 0.0712$ N m^{-1} at 30° C,[42] $e = 1.602 \times 10^{-19}$ C, and the radius r ($r = r_0$ for nascent droplets). Throughout their life cycle (Figure 4), the shrinking droplets remain close to z_R[14, 15, 78] due to their ability to shed charge in the form of small progeny droplets, and/or by IEM ejection of charge carriers.[13, 16, 77] Thus, the net droplet charge can be approximated by eq. 5 not only for nascent droplets, but for all droplets in the ESI plume.[13]

(iv) Nascent Droplet pH. The net charge of the nascent droplets is caused by H^+ from eq. 1.[13, 52] From eq. 5 it follows that the concentration of excess H^+ added to the nascent droplets is $[H^+]_{added} = z_R N_A^{-1} V_0^{-1}$ (Table 1), with Avogadro's number N_A and the initial droplet volume V_0.[13, 55] The pH of shrinking ESI droplets consisting of pure water (without NH_4Ac, for $V \leq V_0$) is therefore

$$pH = -\log (z_R N_A^{-1} V^{-1}) \qquad (6)$$

Eq. 6 predicts that nascent droplets consisting of pure water have pH 4.57 and pH 3.07 for regular ESI and nanoESI, respectively (Table 1, Figure S3B).[40] How does NH_4Ac affect the nascent droplet pH? The production of protons in the ESI source (eq. 1) is equivalent to addition of strong acid, such that eq. 4 can be used for calculating the pH of the NH_4Ac-containing nascent droplets, by substituting $[Cl^-]$ with $z_R N_A^{-1} V_0^{-1}$ (Table 1).

Table 1. Calculated pH of nascent ESI droplets produced from solutions initially at pH 7, after addition of electrolytically generated protons (eq. 1).

NH_4Ac concentration C_0	regular ESI r_0 = 1500 nm $[H^+]_{added}$ = 0.0269 mM	nanoESI r_0 = 150 nm $[H^+]_{added}$ = 0.851 mM
0 mM (pure water) [a]	4.57	3.07
10 mM [b]	6.83	5.75
100 mM [b]	6.98	6.59

(a) from eq. 5; (b) from eq. 4

Table 1 reveals that acidification of the nascent droplets is much less dramatic for NH_4Ac solutions than for pure water. The capability of NH_4Ac to mitigate the effects of protons from eq. 1 may seem surprising, considering that the buffering capacity of NH_4Ac in the neutral range is minimal (note the steep slope at pH 7 in Figure 1). However, although NH_4Ac is not technically a buffer at pH 7,[40, 41] it reduces the extent of acidification by converting free protons from eq. 1 into the weak acid HAc.

$$Ac^- + H^+ \rightleftarrows HAc \qquad K = K_a(HAc)^{-1} = 5.75 \times 10^5 \qquad (7)$$

(v) Charge-Carriers in NH_4Ac-containing ESI Droplets. Excess H^+ from eq. 1 provide nascent droplets with their net charge,[55] but these H^+ get effectively removed by binding to Ac^- and forming HAc (eq. 7). Thus, NH_4^+ ions become the excess charge carriers because their counterions (Ac^-) get converted to neutral HAc. Because pH < 7, these NH_4^+ act as spectator ions that do not affect pH. Instead, the droplet pH is governed by the $[Ac^-]$:[HAc] ratio via eq. 3.

Estimating the pH of Shrinking Droplets While Ignoring NH_4Ac Volatility. The above cornerstones allow us to provide initial estimates of the droplet behavior in the ESI plume. Let us first conduct a thought experiment that disregards the volatile nature of NH_4Ac. Under such conditions, water evaporation will ensure a constant $[Ac^-]$:[HAc] ratio in the shrinking droplets, starting from the nascent conditions of Table 1. Eq. 3 dictates that under these hypothetical conditions the droplets will maintain their nascent near-neutral pH all the way to dryness (Figure S3C, D). Sadly, the next section reveals that this thought experiment is unrealistic because (as stated at the outset), it neglects the implications of NH_3 and HAc evaporation.

Tracking pH in Bulk Evaporation Experiments. How does the volatility of NH_4Ac affect the droplet pH? One might naïvely expect that pH decreases because $NH_4^+(aq) \rightarrow NH_3(g) + H^+(aq)$ releases protons into the droplet. On the other hand, $Ac^-(aq) + H^+(aq) \rightarrow HAc(g)$ might increase pH by removing protons. Thus, in the absence of additional information, it is difficult to predict if the pH of evaporating ESI droplets will go up or down.

To elucidate the implications of NH_4Ac volatility, we tracked the evaporation of bulk samples, while ensuring that the initial solutions matched those of nascent ESI droplets (Table 1). Experiments were conducted on 100 mM and 10 mM aqueous NH_4Ac with an initial pH of 7. The effects of electrolytically generated protons (eq. 1) were captured by adding HCl to these pH 7 solutions, prior to commencing evaporation. HCl concentrations were chosen as $[H^+]_{added} = z_R N_A^{-1} V_0^{-1}$ (eq. 5), where the nascent droplet volume V_0 corresponds to r_0 = 1500 nm (regular ESI) or r_0 = 150 nm (nanoESI). The resulting solution pH agreed with the predicted values of Table 1 within 0.05 units. The composition of all four solutions was then monitored during evaporation. Intriguingly, all samples showed acidification down to pH values between 5.5 and 5.3 (Figures 5A, C, and S4A, C). Extrapolating from these bulk solution data to NH_4Ac-containing ESI droplets, we

conclude: (i) Electrolytically generated protons convert neutral analyte solution into mildly acidic nascent ESI droplets. (ii) For both regular ESI and nanoESI, the evaporating droplets in the ESI plume subsequently undergo additional acidification down to pH 5.4 ± 0.1.

Acid/Base Equilibria in Evaporating NH_4Ac Solutions. To understand the observed acidification (Figures 5A, C, and S4A, C), one has to consider eqs 8 - 10, as well as their sum (eq 11):

$$NH_4^+(aq) \rightleftarrows NH_3(aq) + H^+(aq) \qquad K_a(NH_4^+) = 10^{-9.25} \qquad (8)$$

$$Ac^-(aq) + H_2O \rightleftarrows HAc(aq) + OH^-(aq) \qquad K_b(Ac^-) = 10^{-9.24} \qquad (9)$$

$$H^+(aq) + OH^-(aq) \rightleftarrows H_2O \qquad K_W^{-1} = 10^{14} \qquad (10)$$

$$NH_4^+(aq) + Ac^-(aq) \rightleftarrows NH_3(aq) + HAc(aq) \qquad K_a(NH_4^+)\, K_b(Ac^-)\, K_W^{-1} = 10^{-4.49} \qquad (11)$$

The listed equilibrium constants imply that NH_3 and HAc form predominantly via eq 11, rather than by water protonation or deprotonation (eqs 8, 9). Eq. 11 also dictates that $[NH_4^+(aq)] = [Ac^-(aq)]$ for bulk solution evaporation from pH 7. The products of eq. 11 can then leave the solution; these processes are irreversible because the bulk solutions (and ESI droplets) are open to the atmosphere.

$$NH_3(aq) \rightarrow NH_3(g) \qquad (12a)$$

$$HAc(aq) \rightarrow HAc(g) \qquad (12b)$$

The acidification observed in our evaporation experiments implies that reaction 12a is faster than 12b, consistent with the fact that NH_3 it is a gas under standard conditions, while HAc is a liquid (albeit a volatile one, evident from its pungent smell). The slower rate of reaction 12b causes HAc to accumulate in the droplet, such that $pH = 4.76 + \log [Ac^-(aq)]/[HAc(aq)]$, according to eq. 3.

NMR spectroscopy was used to track $[Ac^-(aq)] + [HAc(aq)]$ concentration by monitoring the CH_3-CO proton signal (Figure S5). During the early stages of evaporation, $[Ac^-(aq)] + [HAc(aq)]$ closely followed the "ideal" profile that would be expected if NH_4Ac were nonvolatile ($[NH_4Ac]_{ideal}$

in Figure S5). However, once the relative solution volume (V_{REL}) approached 0.1, the measured concentrations were noticeably lower than $[NH_4Ac]_{ideal}$. Averaged over all four data sets, 27% of the Ac^- had left the solution as HAc(g) via eq. 12b at V_{REL}= 0.1 (Figure S5).

From the measured pH values (Figures 5A, 5C, S4A and S4C), one can use eq. 3 to decompose the Figure S5 data into separate [HAc] and $[Ac^-]$ contributions, with $[NH_3] \approx 0$ (eq. 3). Also, because $[H^+]_{addded} << C_0$, we can approximate that $[NH_4^+] \approx [Ac^-]$ (eq. 11, Table 1). Concentrations obtained in this way are depicted in Figure 5B for solutions mimicking regular ESI with C_0 = 100 mM. HAc accumulation is clearly apparent in this profile. Similar observations were made for the other three solution conditions (Figures 5D and S4B, D). Once reaching V_{REL} = 0.1, the $[NH_4^+](aq)$ values were 40% lower on average than the corresponding $[NH_4Ac]_{ideal}$, implying that 40% of the NH_4^+ had been converted to NH_3(g) via eq. 11 and left the solution via eq. 12a.

In summary, the evaporation of NH_4Ac solutions under native ESI-mimicking conditions proceeds as follows: Volume changes are due primarily to water evaporation. Proton transfer from NH_4^+ to Ac^- generates NH_3 and HAc in a 1:1 ratio; for V_{REL} = 0.1, 40% of the total NH_4Ac has been converted via this process. Due to its high volatility, all of the NH_3 evaporates immediately (eq. 12a). Because it is less volatile, only ~2/3 (27/40) of the HAc evaporates, while ~1/3 (13/40) of the HAc stays behind and acidifies the solutions down to pH 5.4 ± 0.1. This pH for V_{REL} = 0.1 was remarkably consistent for both regular and nanoESI with 10 or 100 mM NH_4Ac.

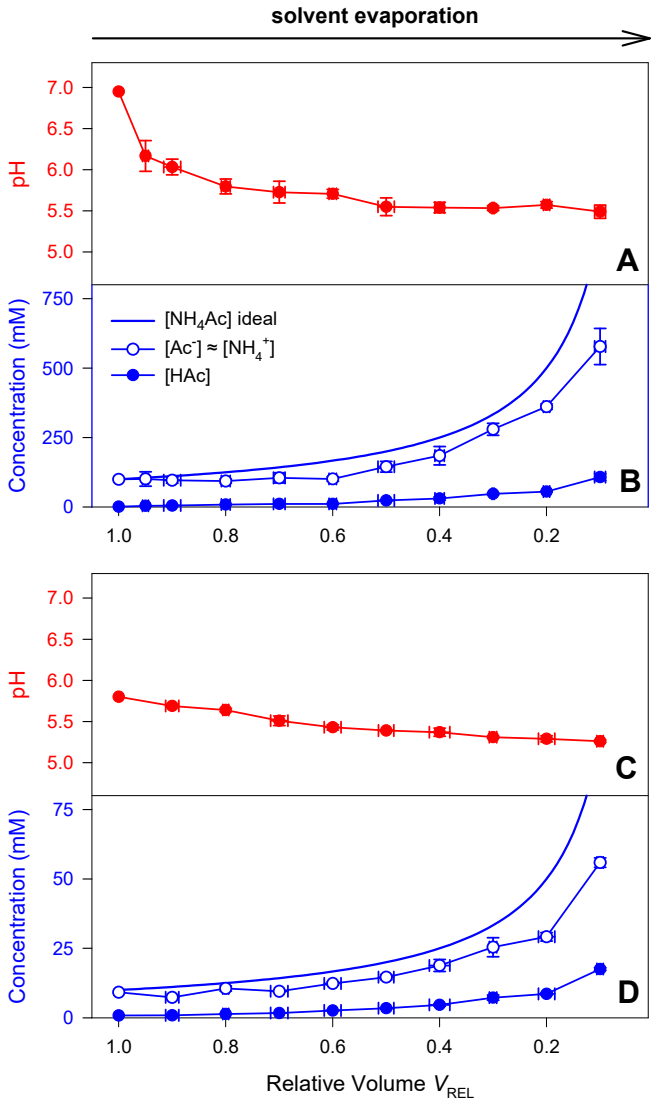

Figure 5. Experimentally measured solution composition during evaporation of bulk aqueous NH_4Ac solutions under ESI-mimicking conditions, starting with the settings of Table 1. (A, B) Regular ESI, r_0 = 1500 nm, C_0 = 100 mM. Panel A shows pH, panel B shows solute concentrations, with $[NH_3](aq) \approx 0$. Also shown is $[NH_4Ac]_{ideal}$, that would be expected if NH_4Ac were nonvolatile. (C, D) Same as in A and B, but for nanoESI with r_0 = 150 nm and C_0 = 10 mM.

As noted, our bulk evaporation experiments were designed to mimic nascent ESI droplets at the Rayleigh limit, consistent with the results of several studies (Table 1).[14, 15, 78] Some reports suggested a lower droplet charge, e.g., ref.[63] reported an average value of $z_{droplet} \approx 0.4 \times z_R$. Nascent droplets will be less acidic under such $z_{droplet} < z_R$ conditions. For example, while Table 1 predicts pH 5.75 for $z_{droplet} = z_R$ in the case of nanoESI with 10 mM NH_4Ac, the corresponding pH would be

6.13 for $z_{droplet} = 0.4 \times z_R$. Luckily, Figures 5 and S4 demonstrate that our key findings are valid for a wide range of nascent pH values, because all NH_4Ac solutions in Table 1 (covering pH 6.98 to 5.75) converged toward pH 5.4 ± 0.1 during evaporation. In other words, the validity of our findings is not limited to conditions where $z_{droplet} = z_R$.

In addition to the experiments of Figures 5, S4, and S5 which covered evaporative concentration enrichment up to ~1 M NH_4Ac, we tested more concentrated solutions to explore the final stages of evaporation. Figure S6 shows data for C_0 = 3.2 M, acidified with HAc to pH 5.5. Evaporation could only be studied down to V_{REL} = 0.25, where the solutions turned into a slurry of precipitated NH_4Ac. Based on the solubility limit of NH_4Ac (~8.3 M)[80] this precipitation should have occurred already at V_{REL} = 0.37, suggesting that ~33% of the NH_4Ac had evaporated at V_{REL} = 0.25. Thus, the extent of NH_4Ac evaporation in highly concentrated samples is comparable to that of the more dilute solutions examined above. Evaporation of the highly concentrated solutions slightly increased pH from 5.5 to 6.2 (Figure S4); however, pH-meter readings under such high salt conditions may not be reliable. Nonetheless, Figure S6 shows that evaporating NH_4Ac solutions do not exhibit any unexpected "erratic" phenomena as they approach the solubility limit.

MD Simulations of NH_4Ac-Containing ESI Droplets. MD has become an important tool for probing ESI mechanisms,[16, 81-89] but there appear to be no previous MD studies on the ESI behavior of NH_4Ac. Proton transfer cannot be modeled using standard MD methods,[70, 90] although this reaction is a key feature of NH_4Ac (eq. 11). Some efforts have been made to conduct MD with proton transfer,[71, 72, 85, 91, 92] but NH_4Ac has not been tackled yet. Here we present a strategy for MD simulations on NH_4Ac-containing ESI droplets. Our approach for the first time considers proton transfer events according to eq. 11, i.e., $NH_4^+ + Ac^- \rightarrow NH_3 + HAc$. Implementation details are

summarized in the SI. Neither H_3O^+ nor OH^- were included in our MD runs, an approximation that is justified by the extremely small equilibrium constants of eqs. 8 and 9.

MD simulations were performed for aqueous droplets with an initial radius of 3 nm, representing a size regime encountered during the final stages in the ESI plume (Figure 4).[13] To account for the concentration enhancement earlier during the droplet life cycle, the runs started with a relatively high NH_4Ac concentration of 1.6 M. Additional NH_4^+ were inserted to bring the droplets to the 19+ Rayleigh limit (eq. 5). Figure 5 implies that NH_4Ac-containing ESI droplets have pH values around 5.4. Accordingly, 0.3 M HAc was added to the MD droplets (eq. 3), for an initial droplet composition of 3050 H_2O, 127 NH_4^+, 108 Ac^-, and 20 HAc. The droplets modeled here were analyte-free, analogous to the experiments of Figure 3C, D. Figure 6A-D shows snapshots of a typical droplet simulation. Water evaporation was accompanied by occasional IEM ejection of solvated NH_4^+.[13, 16, 77, 93] NH_3 and HAc evaporated as individual molecules without solvation shell. After 75 ns the droplet had vanished, leaving behind a tiny $[NH_3 + NH_4]^+$ ion (Figure 6D).

Figure 7 takes a closer look at time-dependent changes under the conditions of Figure 6A-D. Water loss went to completion within ~20 ns (Figure 7A). Concomitant with this evaporation, the droplet lost NH_3(g) and HAc(g) after their production by proton transfer (Figure 7B, C). Although these two neutrals were formed in a 1:1 ratio, the NH_3 concentration remained five to ten times lower than that of HAc, because the former showed a higher evaporation propensity (Figure 7B). The higher volatility of NH_3 relative to HAc seen in these simulations is consistent with the bulk experiments of Figure 5. Gradual solvent loss increased the NH_4^+ and Ac^- concentrations to ~ 8 M (Figure 7D), which is the solubility limit of NH_4Ac.[80] The droplet charge oscillated around 81% of the Rayleigh limit, resulting from the interplay of evaporative droplet shrinkage and NH_4^+ IEM ejection (Figure 7E). This z/z_R regime is similar to previous simulation data involving H^+ or Na^+,[71] in line with experiments.[14, 62] From the Ac^-/HAc ratio in Figure 7B, one can calculate the average

droplet pH via eq. 3. Figure 7E illustrates that this pH stays in the range of 5.1-5.7, close to the measured bulk value of 5.4 ± 0.1 (Figure 5). We conclude that the MD strategy developed here yields simulated data that are consistent with a wide range of experimental observations.

Inspection of the MD droplets revealed that Ac^- and NH_4^+ preferentially reside in the droplet interior, whereas HAc underwent surface enrichment with the methyl groups pointing into the vapor phase (Figure S7). In other words, the droplet surface has a lower Ac^-/HAc ratio than the interior, implying that the surface of NH_4Ac-containing ESI droplets is more acidic than the interior (eq 3).

Volatile vs. Nonvolatile Salts. One can compare the NH_4Ac data of Figure 6A-D with results for a typical nonvolatile salt such as NaCl. Figure 6E-H shows MD data for an ESI droplet containing 1.6 M NaCl. Evaporation of this droplet produced a large $Na_nCl_m^{(n-m)+}$ CRM cluster. Details of the NaCl droplet behavior can be found in ref. [72]. Figure 6 strikingly illustrates the difference between a volatile and a nonvolatile salt during ESI. In the former case, solvent and solutes evaporate until there is virtually nothing left (Figure 6D), whereas the latter scenario produces large CRM clusters (Figure 6H). These MD data mirror the experiments of Figure 3, where ESI of NaCl solution generated adducts and clusters, whereas such interferences were absent for NH_4Ac solution.

The key ingredient of our NH_4Ac simulations was the implementation of a strategy that allowed for proton transfer from NH_4^+ to Ac^-. MD runs conducted without this proton transfer produced large NH_4Ac clusters (Figure S8), akin to the NaCl behavior Figure 6E-H. Figure S8 demonstrates that neither NH_4^+ nor Ac^- are volatile *per se*. Instead, these ions become volatile only after converting to neutrals by proton transfer (see TOC Figure). Traditional MD methods that do not allow for proton transfer[94] are therefore unsuitable for modeling the ESI behavior of NH_4Ac.

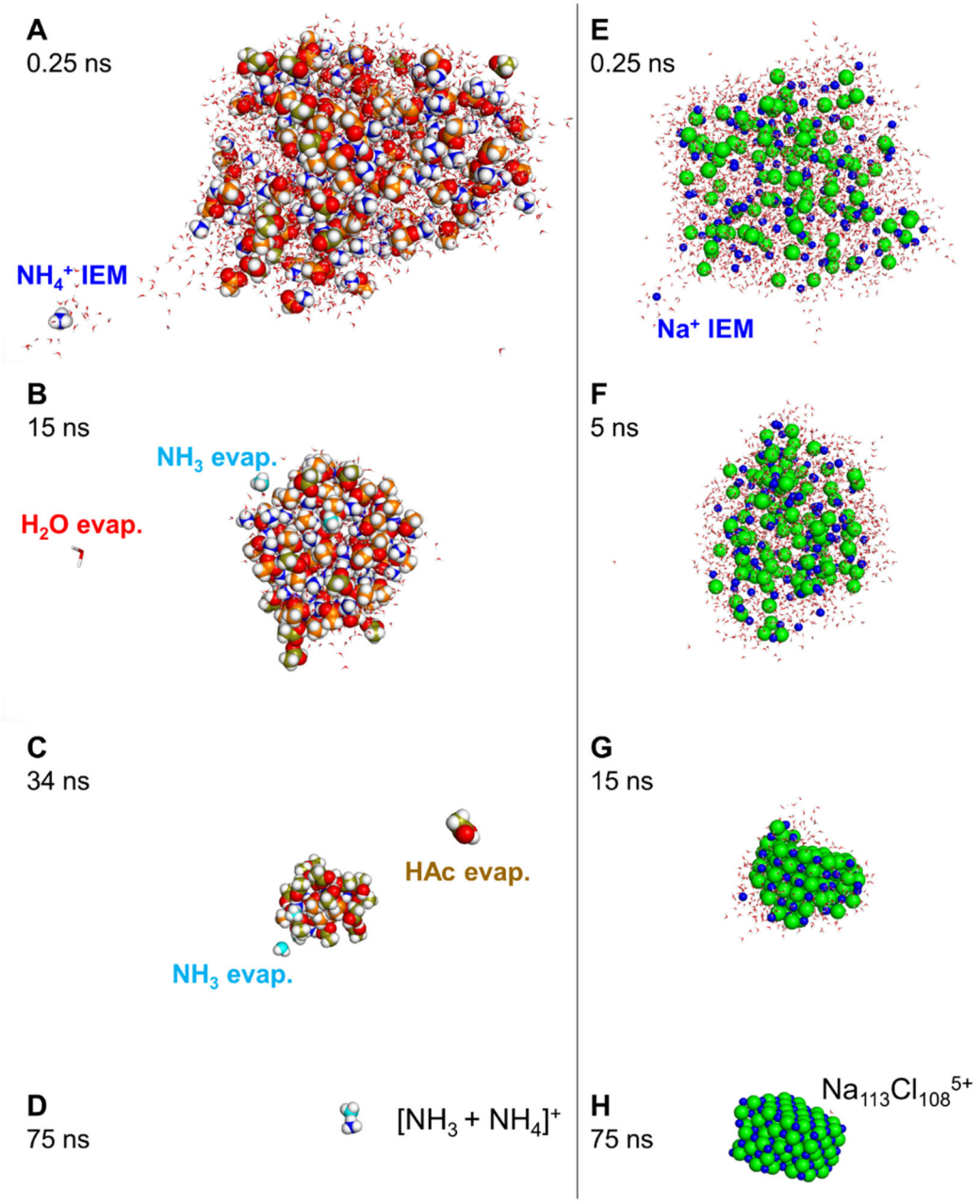

Figure 6. MD snapshots of Rayleigh-charged aqueous ESI droplets, initially containing 1.6 M salt. (A-D) NH_4Ac-containing droplet with $NH_4^+ + Ac^- \rightarrow NH_3 + HAc$ proton transfer. IEM ejection of NH_4^+, and evaporation events of NH_3, HAc, and H_2O are highlighted. (E-H) NaCl-containing droplet under conditions that were otherwise identical to those of panels A-D. Coloring; Na^+ (blue) Cl^- (green), NH_4^+ nitrogen (blue), NH_3 nitrogen (cyan), Ac^- carbon (orange), HAc carbon (olive), O (red), H (white). Solute atoms are shown as spheres, H_2O as red sticks.

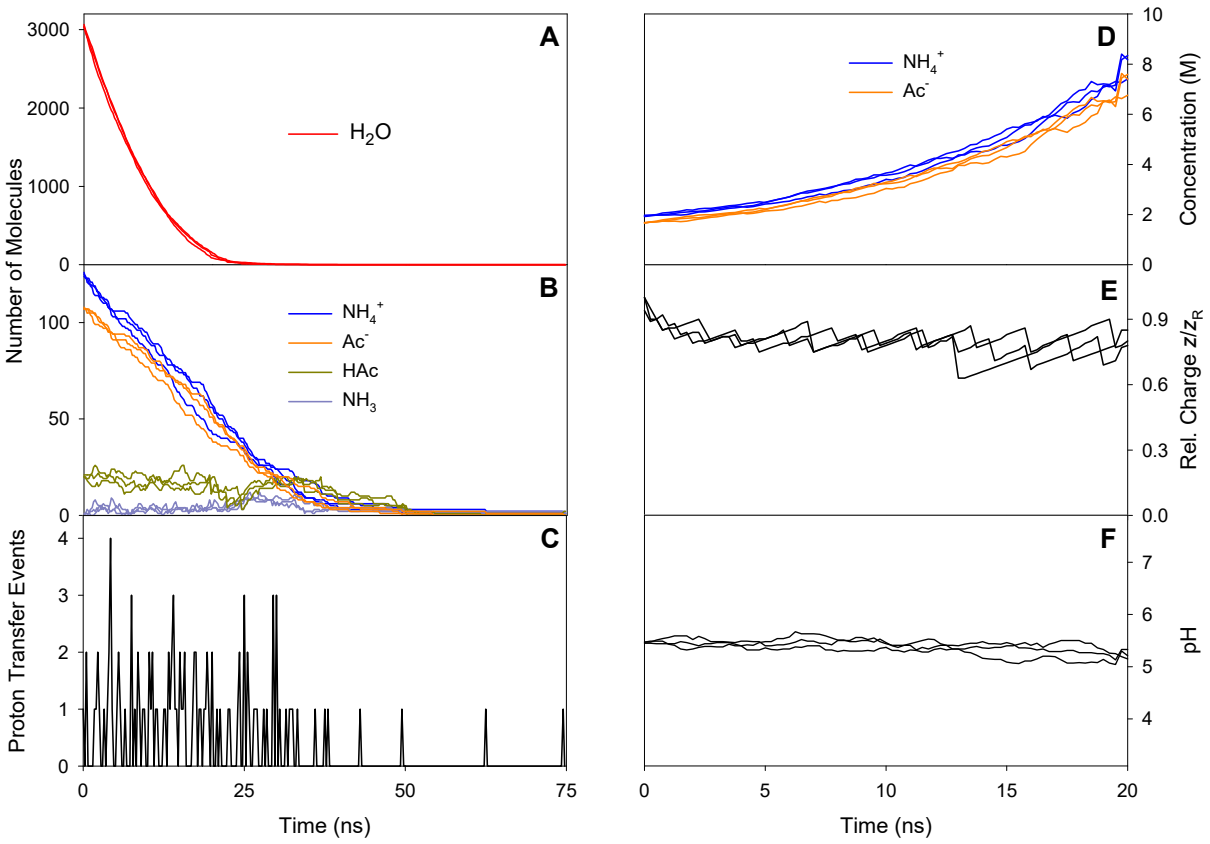

Figure 7. MD-simulated changes in the composition of aqueous NH_4Ac droplets under the conditions of Figure 6A-D. (A, B) Number of water and solute molecules. (C) Number of proton transfer events per 250 ps interval. (D) Concentration of NH_4^+ and Ac^-. (E) Droplet charge relative to the Rayleigh limit. (F) pH. Note the different time range in panels A-C vs. D-F, reflecting the fact that the properties displayed in D-F are only meaningful for aqueous solutions. All panels contain data from triplicate MD runs; only panel C shows a single run to prevent cluttering.

Conclusions

Although NH_4Ac is a standard additive in native ESI, little is known about the environment experienced by analytes after their entrapment in nascent droplets, and during the subsequent events in the ESI plume. The current work clears up some of these uncertainties. Ideally, biomolecular analytes would be subjected to pH 7 up until the point when they are released from ESI nanodroplets into the gas phase. Inadvertent acidification and other destabilizing factors can alter the properties of analytes and affect the resulting mass spectra.[27, 44-53]

The findings of this work imply that ESI droplets formed from NH_4Ac-containing aqueous solution with an initial pH of 7 experience two stages of acidification. The first stage occurs when nascent droplets formed at the tip of the Taylor cone acquire a net charge close to the Rayleigh limit by electrolytically produced H^+. More precisely, these H^+ appear in aqueous solution as H_3O^+, which represents the strongest acid that can stably exist in water.[56] NH_4Ac does not match the textbook definition of a buffer,[41] but it mitigates the effects of these H_3O^+ by converting them to HAc which is a weak acid (eq. 7). The use of relatively high NH_4Ac concentrations (e.g. 100 mM instead of 10 mM) will ensure that nascent ESI droplets retain a near-neutral pH (Table 1).

NH_4Ac decomposes into two volatile components (NH_3 and HAc), allowing the formation of adduct-free biomolecular ions during ESI.[13] The current work uncovered that this volatility has an unanticipated flipside, as it gives rise to a second stage of acidification. The fact that NH_3 evaporates from the droplet more quickly than HAc causes the latter to accumulate in the droplet. As a result, the NH_4Ac solution turns into an acetate (Ac^-/HAc) buffer with a pH that is governed by eq. 3. Our data suggest that the evaporating droplets approach pH of 5.4 ± 0.1, regardless of the initial NH_4Ac concentration for both regular and nanoESI.

Although pH 5.4 does not represent a physiological environment, many globular proteins maintain their native conformation in bulk solution under these conditions.[95, 96] Even for biomolecular analytes that are unstable at this pH, one has to consider that pH-induced changes take time. For example, protein unfolding in solution typically takes place on time scales of milliseconds to seconds,[97] while the ESI events of Figure 4 occur within a millisecond or less.[13, 69] Thus, pH-sensitive analytes may survive the ESI process unscathed simply because the acidic droplet environment persists only for a short time interval[98] (although the possibility of unfolding in droplets has been demonstrated for some proteins[53]). Overall, NH_4Ac is not a perfect pH stabilizer for native ESI, but it appears to be "good enough" for many applications, as demonstrated by the numerous

successful studies that have used this additive.[1-12] Possible alternatives come with their own problems, e.g., ammonium bicarbonate can promote protein unfolding and cross-linking.[99, 100]

In addition to our experimental and conceptual findings, the current work demonstrated the viability of conducting MD simulations on NH_4Ac-containing ESI droplets. For the first time, we implemented an MD algorithm that considers the volatile nature of this salt by allowing for proton transfer. These simulations yielded data that supported our bulk solution experiments, in particular, the high volatility of NH_3 and the formation of a Ac^-/HAc buffer in the evaporating droplets. We are currently extending these simulations to ESI droplets containing proteins and other biomolecular analytes, to obtain a truly molecular understanding of native ESI. The results of these endeavors will be reported elsewhere.

Acknowledgements. We thank Pablo Scrosati for help with the Linux computers used in this work. Marcin Borkowski (https://www.chembuddy.com) is acknowledged for input related to eq. 2.

Supporting Information. Derivation of Equation 2, Figure S1: NMR spectra of NH_4Ac at different pH, Complete Computational Methods, Figure S2: Molecular geometry of $NH_4^+ + Ac^- \rightarrow NH_3 +$ HAc proton transfer, Figure S3: Estimated properties of Rayleigh-charged ESI droplets, Figure S4: Bulk solution evaporation for regular ESI at 10 mM and nanoESI at 100 mM NH_4Ac, Figure S5: NMR-detected NH_4Ac concentration in evaporating bulk solution, Figure S6: Bulk solution evaporation for highly concentrated NH_4Ac solution, Figure S7: MD data of HAc enrichment at the droplet surface, Figure S8: MD snapshots for an aqueous NH_4Ac droplet without proton transfer.

References

(1) Tamara, S.; den Boer, M. A.; Heck, A. J. R. High-Resolution Native Mass Spectrometry. *Chem. Rev.* **2022**, 122, 7269-7326.

(2) Mehmood, S.; Allison, T. M.; Robinson, C. V. Mass Spectrometry of Protein Complexes: From Origins to Applications. *Annu. Rev. Phys. Chem.* **2015**, 66, 453-474.

(3) Christofi, E.; Barran, P. Ion Mobility Mass Spectrometry (IM-MS) for Structural Biology: Insights Gained by Measuring Mass, Charge, and Collision Cross Section. *Chem. Rev.* **2023**, 123, 2902–2949.

(4) Yang, Y.; Niu, C. D.; Bobst, C. E.; Kaltashov, I. A. Charge Manipulation Using Solution and Gas-Phase Chemistry to Facilitate Analysis of Highly Heterogeneous Protein Complexes in Native Mass Spectrometry. *Anal. Chem.* **2021**, 93, 3337-3342.

(5) Khristenko, N.; Rosu, F.; Largy, E.; Haustant, J.; Mesmin, C.; Gabelica, V. Native Electrospray Ionization of Multi-Domain Proteins via a Bead Ejection Mechanism. *J. Am. Chem. Soc.* **2023**, 145, 498–506.

(6) Bui, D. T.; Li, Z. X.; Kitov, P. I.; Han, L.; Kitova, E. N.; Fortier, M.; Fuselier, C.; Boissel, P.; Chatenet, D.; Doucet, N.; Tompkins, S. M.; St-Pierre, Y.; Mahal, L. K., et al. Quantifying Biomolecular Interactions Using Slow Mixing Mode (SLOMO) Nanoflow ESI-MS. *ACS Central Sci.* **2022**, 8, 963-974.

(7) Deslignière, E.; Ollivier, S.; Beck, A.; Ropartz, D.; Rogniaux, H.; Cianférani, S. Benefits and Limitations of High-Resolution Cyclic IM-MS for Conformational Characterization of Native Therapeutic Monoclonal Antibodies. *Anal. Chem.* **2023**, 95, 4162-4171.

(8) Schneeberger, E.-M.; Halper, M.; Palasser, M.; Heel, S. V.; Vušurović, J.; Plangger, R.; Juen, M.; Kreutz, C.; Breuker, K. Native mass spectrometry reveals the initial binding events of HIV-1 rev to RRE stem II RNA. *Nat. Commun.* **2020**, 11, 5750.

(9) Zhou, M. W.; Lantz, C.; Brown, K. A.; Ge, Y.; Pasa-Tolic, L.; Loo, J. A.; Lermyte, F. Higher-order structural characterisation of native proteins and complexes by top-down mass spectrometry. *Chem. Sci.* **2020**, 11, 20.

(10) Morrison, L. J.; Brodbelt, J. S. 193 nm Ultraviolet Photodissociation Mass Spectrometry of Tetrameric Protein Complexes Provides Insight into Quaternary and Secondary Protein Topology. *J. Am. Chem. Soc.* **2016**, 138, 10849-10859.

(11) Snyder, D. T.; Harvey, S. R.; Wysocki, V. H. Surface-induced Dissociation Mass Spectrometry as a Structural Biology Tool. *Chem. Rev.* **2022**, 122, 7442-7487.

(12) Bonner, J. G.; Lyon, Y. A.; Nellessen, C.; Julian, R. R. Photoelectron Transfer Dissociation Reveals Surprising Favorability of Zwitterionic States in Large Gaseous Peptides and Proteins. *J. Am. Chem. Soc.* **2017**, 139, 10286-10293.

(13) Kebarle, P.; Verkerk, U. H. Electrospray: From Ions in Solutions to Ions in the Gas Phase, What We Know Now. *Mass Spectrom. Rev.* **2009**, 28, 898-917.

(14) Grimm, R. L.; Beauchamp, J. L. Evaporation and Discharge Dynamics of Highly Charged Multicomponent Droplets Generated by Electrospray Ionization. *J. Phys. Chem. A* **2010**, 114, 1411-1419.

(15) Harper, C. C.; Brauer, D. D.; Francis, M. B.; Williams, E. R. Direct observation of ion emission from charged aqueous nanodrops: effects on gaseous macromolecular charging. *Chem. Sci.* **2021**, 12, 5185-5195.

(16) Aliyari, E.; Konermann, L. Formation of Gaseous Proteins via the Ion Evaporation Model (IEM) in Electrospray Mass Spectrometry. *Anal. Chem.* **2020**, 92, 10807-10814.

(17) Wyttenbach, T.; Bowers, M. T. Structural Stability from Solution to the Gas Phase: Native Solution Structure of Ubiquitin Survives Analysis in a Solvent-Free Ion Mobility–Mass Spectrometry Environment. *J. Phys. Chem. B* **2011**, 115, 12266-12275.
(18) Bleiholder, C.; Liu, F. C. Structure Relaxation Approximation (SRA) for Elucidation of Protein Structures from Ion Mobility Measurements. *J. Phys. Chem. B* **2019**, 123, 2756-2769.
(19) Kit, M. C. S.; Webb, I. K. Application of Multiple Length Cross-linkers to the Characterization of Gaseous Protein Structure. *Anal. Chem.* **2022**, 94, 13301−13310.
(20) Zercher, B. P.; Hong, S.; Roush, A. E.; Feng, Y. Q.; Bush, M. F. Are the Gas-Phase Structures of Molecular Elephants Enduring or Ephemeral? Results from Time-Dependent, Tandem Ion Mobility. *Anal. Chem.* **2023**, 95, 9589–9597.
(21) Creighton, T. E. *Proteins*; W. H. Freeman & Co: New York, 1993.
(22) Deutsch, C.; Taylor, J. S.; Wilson, D. F. Regulation of intracellular pH by human peripheral blood lymphocytes as measured by 19F NMR. *Proc. Natl. Acad. Sci. U.S.A.* **1982**, 79, 7944-7948.
(23) Boron, W. F. Regulation of intracellular pH. *Adv. Physiol. Educ.* **2004**, 28, 160-179.
(24) Cleary, S. P.; Prell, J. S. Liberating Native Mass Spectrometry from Dependence on Volatile Salt Buffers by Use of Gabor Transform. *Chemphyschem* **2019**, 20, 519-523.
(25) Xu, N.; Lin, Y.; Hofstadler, S. A.; Matson, D.; Call, C. J.; Smith, R. D. A Microfabricated Dialysis Device for Sample Cleanup in Electrospray Ionization Mass Spectrometry. *Anal. Chem.* **1998**, 70, 3553-3556.
(26) de la Mora, J. F. Electrospray Ionization of large multiply charged species proceeds via Dole's charged residue mechanism. *Anal. Chim. Acta* **2000**, 406, 93-104.
(27) Kitova, E. N.; El-Hawiet, A.; Schnier, P. D.; Klassen, J. S. Reliable Determinations of Protein–Ligand Interactions by Direct ESI-MS Measurements. Are We There Yet? *J. Am. Soc. Mass Spectrom.* **2012**, 23, 431-441.
(28) Susa, A. C.; Xia, Z. J.; Williams, E. R. Native Mass Spectrometry from Common Buffers with Salts That Mimic the Extracellular Environment. *Angew. Chem.-Int. Edit.* **2017**, 56, 7912-7915.
(29) Nguyen, G. T. H.; Tran, T. N.; Podgorski, M. N.; Bell, S. G.; Supuran, C. T.; Donald, W. A. Nanoscale Ion Emitters in Native Mass Spectrometry for Measuring Ligand–Protein Binding Affinities. *ACS Centr. Sci.* **2019**, 5, 308–318.
(30) Jordan, J. S.; Xia, Z.; Williams, E. R. Tips on Making Tiny Tips: Secrets to Submicron Nanoelectrospray Emitters. *J. Am. Soc. Mass Spectrom.* **2022**, 33, 607-611.
(31) Harvey, S. R.; VanAernum, Z. L.; Wysocki, V. H. Surface-Induced Dissociation of Anionic vs Cationic Native-Like Protein Complexes. *J. Am. Chem. Soc.* **2021**, 143, 7698-7706.
(32) Walker, T. E.; Laganowsky, A.; Russell, D. H. Surface Activity of Amines Provides Evidence for the Combined ESI Mechanism of Charge Reduction for Protein Complexes. *Anal. Chem.* **2022**, 94, 10824-10831.
(33) Ghosh, D. K.; Rosu, F.; Gabelica, V. Negative Electrospray Supercharging Mechanisms of Nucleic Acid Structures. *Anal. Chem.* **2022**, 94, 15386–15394.
(34) Woodall, D. W.; Henderson, L. W.; Raab, S. A.; Honma, K.; Clemmer, D. E. Understanding the Thermal Denaturation of Myoglobin with IMS-MS: Evidence for Multiple Stable Structures and Trapped Pre-equilibrium States. *J. Am. Soc. Mass Spectrom.* **2021**, 32, 64-72.
(35) May, J. C.; Jurneczko, E.; Stow, S. M.; Kratochvil, I.; Kalkhof, S.; McLean, J. A. Conformational landscapes of ubiquitin, cytochrome c, and myoglobin: Uniform field ion

mobility measurements in helium and nitrogen drift gas. *Int. J. Mass Spectrom.* **2018**, 427, 79-90.
(36) Gavriilidou, A. F. M.; Gulbakan, B.; Zenobi, R. Influence of Ammonium Acetate Concentration on Receptor Ligand Binding Affinities Measured by Native Nano ESI-MS: A Systematic Study. *Anal. Chem.* **2015**, 87, 10378-10384.
(37) Gumerov, D. R.; Dobo, A.; Kaltashov, I. A. Protein-ion charge-state distributions in electrospray ionization mass spectrometry: distinguishing conformational contributions from masking effects. *Eur. J. Mass Spectrom.* **2002**, 8, 123-129.
(38) Abzalimov, R. R.; Dubin, P. L.; Kaltashov, I. A. Glycosaminoglycans as Naturally Occurring Combinatorial Libraries: Developing a Mass Spectrometry-Based Strategy for Characterization of Anti-Thrombin Interaction with Low Molecular Weight Heparin and Heparin Oligomers. *Anal. Chem.* **2007**, 79, 6055-6063.
(39) Williams, R. J.; Lyman, C. M. A Neutral Buffered Standard for Hydrogen Ion Work and Accurate Titrations Which Can be Prepared in One Minute. *J. Am. Chem. Soc.* **1932**, 54, 1911-1912.
(40) Konermann, L. Addressing a Common Misconception: Ammonium Acetate as Neutral pH "Buffer" for Native Electrospray Mass Spectrometry. *J. Am. Soc. Mass Spectrom.* **2017**, 28, 1827-1835.
(41) Masterton, W. L.; Hurley, C. N. *Chemistry, Principles and Reactions*, 6th ed.; Brooks/Cole Cengage Learning, 2009.
(42) Lide, D. R. *CRC Handbook of Chemistry and Physics*, 82nd ed.; CRC Press: Boca Raton, London, New York, Washington, 2001.
(43) Naiman, B. The Bronsted concept of acids and bases in quantitative analysis. *J. Chem. Ed.* **1948**, 25, 454.
(44) Konermann, L.; Silva, E. A.; Sogbein, O. F. Electrochemically Induced pH Changes Resulting in Protein Unfolding in the Ion Source of an Electrospray Mass Spectrometer. *Anal. Chem.* **2001**, 73, 4836-4844.
(45) Wang, F.; Tang, X. Conformational Heterogeneity and Stability of Apomyoglobin Studied by Hydrogen/Deuterium Exchange and Electrospray Ionization Mass Spectrometry. *Biochemistry* **1996**, 35, 4069-4078.
(46) Plonka, D.; Kotuniak, R.; Dabrowska, K.; Bal, W. Electrospray-Induced Mass Spectrometry Is Not Suitable for Determination of Peptidic Cu(II) Complexes. *J. Am. Soc. Mass Spectrom.* **2021**, 32, 2766-2776.
(47) Gatlin, C. L.; Turecek, F. Acidity Determination in Droplets Formed by Electrospraying Methanol-Water Solutions. *Anal. Chem.* **1994**, 66, 712-718.
(48) McDonald, L. W.; Campbell, J. A.; Clark, S. B. Failure of ESI Spectra to Represent Metal-Complex Solution Composition: A Study of Lanthanide-Carboxylate Complexes. *Anal. Chem.* **2014**, 86, 1023-1029.
(49) Wang, H.; Agnes, G. R. Kinetically Labile Equilibrium Shifts Induced by the Electrospray Process. *Anal. Chem.* **1999**, 71, 4166-4172.
(50) Zhang, M. X.; Gumerov, D. R.; Kaltashov, I. A.; Mason, A. B. Indirect detection of protein-metal binding: Interaction of serum transferrin with In3+ and Bi3+. *J. Am. Soc. Mass Spectrom.* **2004**, 15, 1658-1664.
(51) Bich, C.; Baer, S.; Jecklin, M. C.; Zenobi, R. Probing the Hydrophobic Effect of Noncovalent Complexes by Mass Spectrometry. *J. Am. Soc. Mass Spectrom.* **2010**, 21, 286-289.
(52) Jecklin, M. C.; Touboul, D.; Bovet, C.; Wortmann, A.; Zenobi, R. Which Electrospray-Based Ionization Method Best Reflects Protein-Ligand Interactions Found in Solution? A

Comparison of ESI, nanoESI, and ESSI for the Determination of Dissociation Constants with Mass Spectrometry. *J. Am. Soc. Mass Spectrom.* **2008**, 19, 332-343.
(53) Kharlamova, A.; Prentice, B. M.; Huang, T.-Y.; McLuckey, S. A. Electrospray Droplet Exposure to Gaseous Acids for the Manipulation of Protein Charge State Distributions. *Anal. Chem.* **2010**, 82, 7422-7429.
(54) Gadzuk-Shea, M. M.; Hubbard, E. E.; Gozzo, T. A.; Bush, M. F. Sample pH Can Drift during Native Mass Spectrometry Experiments: Results from Ratiometric Fluorescence Imaging. *J. Am. Soc. Mass Spectrom.* **2023**, 34, in press.
(55) Van Berkel, G. J.; Kertesz, V. Using the Electrochemistry of the Electrospray Ion Source. *Anal. Chem.* **2007**, 79, 5511-5520.
(56) Eigen, M. Proton Transfer, Acid-Base Catalysis, and Enzymatic Hydrolysis. *Angew. Chem.-Int. Edit.* **1964**, 3, 1-72.
(57) Zhou, S.; Prebyl, B. S.; Cook, K. D. Profiling pH Changes in the Electrospray Plume. *Anal. Chem.* **2002**, 74, 4885-4888.
(58) Girod, M.; Dagany, X.; Antoine, R.; Dugourd, P. Relation between charge state distributions of peptide anions and pH changes in the electrospray plume. A mass spectrometry and optical spectroscopy investigation. *Int. J. Mass Spectrom.* **2011**, 308, 41-48.
(59) Malevanets, A.; Consta, S. Variation of droplet acidity during evaporation. *J. Chem. Phys.* **2013**, 138, 184312.
(60) Van Berkel, G. J.; Asano, K. G.; Schnier, P. D. Electrochemical Processes in a Wire-in-a-Capillary Bulk-Loaded, Nano-Electrospray Emitter. *J. Am. Soc. Mass Spectrom.* **2001**, 12, 853-862.
(61) Nemes, P.; Marginean, I.; Vertes, A. Spraying Mode Effect on Droplet Formation and Ion Chemistry in Electrosprays. *Anal. Chem.* **2007**, 79, 3105-3116.
(62) Cooper, R. J.; O'Brien, J. T.; Chang, T. M.; Williams, E. R. Structural and electrostatic effects at the surfaces of size- and charge-selected aqueous nanodrops. *Chem. Sci.* **2017**, 8, 5201-5213.
(63) Mabbett, S. R.; Zilch, L. W.; Maze, J. T.; Smith, J. W.; Jarrold, M. F. Pulsed Acceleration Charge Detection Mass Spectrometry: Application to Weighing Electrosprayed Droplets. *Anal. Chem.* **2007**, 79, 8431-8439.
(64) Wang, R.; Zenobi, R. Evolution of the Solvent Polarity in an Electrospray Plume. *J. Am. Soc. Mass Spectrom.* **2010**, 21, 378-385.
(65) Gibson, S. C.; Feigerle, C. S.; Cook, K. D. Fluorometric Measurement and Modeling of Droplet Temperature Changes in an Electrospray Plume. *Anal. Chem.* **2014**, 86, 464-472.
(66) Westphall, M. S.; Jorabchi, K.; Smith, L. M. Mass spectrometry of acoustically levitated droplets. *Anal. Chem.* **2008**, 80, 5847-5853.
(67) Wilm, M.; Mann, M. Analytical Properties of the Nanoelectrospray Ion Source. *Anal. Chem.* **1996**, 68, 1-8.
(68) Baldwin, W. G.; Burchill, C. E. Equilibrium Constants for Water and Hydronium Ion. *J. Chem. Educ.* **1987**, 64, 1067-1067.
(69) Kebarle, P.; Tang, L. From ions in solution to ions in the gas phase: The mechanism of electrospray mass spectrometry. *Anal. Chem.* **1993**, 65, 972A-986A.
(70) Abraham, M. J.; Murtola, T.; Schulz, R.; Páll, S.; Smith, J. C.; Hess, B.; Lindahl, E. GROMACS: High performance molecular simulations through multi-level parallelism from laptops to supercomputers. *SoftwareX* **2015**, 1–2, 19-25.
(71) Konermann, L.; Kim, S. Grotthuss Molecular Dynamics Simulations for Modeling Proton Hopping in Electrosprayed Water Droplets. *J. Chem. Theo. Comp.* **2022**, 18, 3781-3794.

(72) Konermann, L.; Haidar, Y. Mechanism of Magic Number NaCl Cluster Formation from Electrosprayed Water Nanodroplets. *Anal. Chem.* **2022**, 94, 16491-16501.
(73) Bunio, L. B.; Wang, J. Y.; Kannaiyan, R.; Gates, I. D. Evaporation and crystallization of NaCl-water droplets suspended in air by acoustic levitation. *Chem. Eng. Sci.* **2022**, 251, 9.
(74) Juraschek, R.; Dulcks, T.; Karas, M. Nanoelectrospray - More than just a Minimized-Flow Electrospray Ionization Source. *J. Am. Soc. Mass Spectrom.* **1999**, 10, 300-308.
(75) Wang, G.; Cole, R. B. Charged residue versus ion evaporation for formation of alkali metal halide clusters ions in ESI. *Anal. Chim. Acta* **2000**, 406, 53-65.
(76) Abian, J.; Sanchezbaeza, F.; Gelpi, E.; Barcelo, D. On the Origin of Some Controversial Ions (m/z 59, 60, 77, and 119) in the Thermospray Reagent Plasma from Ammonium Acetate. *J. Am. Soc. Mass Spectrom.* **1994**, 5, 186-193.
(77) Iribarne, J. V.; Thomson, B. A. On the evaporation of small ions from charged droplets. *J. Chem. Phys.* **1976**, 64, 2287-2294.
(78) Gomez, A.; Tang, K. Charge and fission of droplets in electrostatic sprays. *Phys. Fluids* **1994**, 6, 404-414.
(79) Wilm, M. S.; Mann, M. Electrospray and Taylor-Cone theory, Dole's beam of macromolecules at last? *Int. J. Mass Spectrom.* **1994**, 136, 167-180.
(80) Iavarone, A. T.; Udekwu, O. A.; Williams, E. R. Buffer Loading for Counteracting Metal Salt-Induced Signal Suppression in Electrospray Ionization. *Anal. Chem.* **2004**, 76, 3944-3950.
(81) Znamenskiy, V.; Marginean, I.; Vertes, A. Solvated Ion Evaporation from Charged Water Droplets. *J. Phys. Chem. A* **2003**, 107, 7406-7412.
(82) Caleman, C.; van der Spoel, D. Evaporation from water clusters containing singly charged ions. *Phys. Chem. Chem. Phys.* **2007**, 9, 5105-5111.
(83) Calixte, E. I.; Liyanage, O. T.; Kim, H. J.; Ziperman, E. D.; Pearson, A. J.; Gallagher, E. S. Release of Carbohydrate-Metal Adducts from Electrospray Droplets: Insight into Glycan Ionization by Electrospray. *J. Phys. Chem. B* **2020**, 124, 479-486.
(84) Kwan, V.; O'Dwyer, R.; Laur, D.; Tan, J. J.; Consta, S. Relation between Ejection Mechanism and Ion Abundance in the Electric Double Layer of Droplets. *J. Phys. Chem. A* **2021**, 125, 2954-2966.
(85) Saintmont, F.; Hoyas, S.; Rosu, F.; Gabelica, V.; Brocorens, P.; Gerbaux, P. Structural Characterization of Dendriplexes In Vacuo: A Joint Ion Mobility/Molecular Dynamics Investigation. *J. Am. Soc. Mass Spectrom.* **2022**, 33, 1555-1568.
(86) Kim, D.; Wagner, N.; Wooding, K.; Clemmer, D. E.; Russell, D. H. Ions from Solution to the Gas Phase: A Molecular Dynamics Simulation of the Structural Evolution of Substance P during Desolvation of Charged Nanodroplets Generated by Electrospray Ionization. *J. Am. Chem. Soc.* **2017**, 139, 2981-2988.
(87) Kondalaji, S. G.; Khakinejad, M.; Valentine, S. J. Comprehensive Peptide Ion Structure Studies Using Ion Mobility Techniques: Part 3. Relating Solution-Phase to Gas-Phase Structures. *J. Am. Soc. Mass Spectrom.* **2018**, 29, 1665-1677.
(88) Wang, B.; Tieleman, D. P. Release of nanodiscs from charged nano-droplets in the electrospray ionization revealed by molecular dynamics simulations. *Commun. Chem.* **2023**, 6, 21.
(89) Luan, M. J.; Hou, Z. H.; Huang, G. M. Suppression of Protein Structural Perturbations in Native Electrospray Ionization during the Final Evaporation Stages Revealed by Molecular Dynamics Simulations. *J. Phys. Chem. B* **2022**, 126, 144−150.

(90) Huang, J.; MacKerell, A. D. CHARMM36 all-atom additive protein force field: Validation based on comparison to NMR data. *J. Comput. Chem.* **2013**, 34, 2135-2145.
(91) Moore, C. C.; Staroverov, V. N.; Konermann, L. Using Density Functional Theory for Testing the Robustness of Mobile-Proton Molecular Dynamics Simulations on Electrosprayed Ions: Structural Implications for Gaseous Proteins. *J. Phys. Chem. B* **2023**, 127, 4061-4071.
(92) Fegan, S. K.; Thachuk, M. A Charge Moving Algorithm for Molecular Dynamics Simulations of Gas-Phase Proteins. *J. Chem. Theory Comput.* **2013**, 9, 2531-2539.
(93) Loscertales, I. G.; de la Mora, J. F. Experiments on the kinetics of field evaporation of small ions from droplets. *J. Chem. Phys.* **1995**, 103, 5041-5060.
(94) Drecun, O.; Striolo, A.; Bernardini, C. Structural and dynamic properties of some aqueous salt solutions. *Phys. Chem. Chem. Phys.* **2021**, 23, 15224-15235.
(95) Goto, Y.; Hagihara, Y.; Hamada, D.; Hoshino, M.; Nishii, I. Acid-Induced Unfolding and Refolding Transitions of Cytochrome c: A Three-State Mechanism in H_2O and D_2O. *Biochemistry* **1993**, 32, 11878-11885.
(96) Fink, A. L.; Calciano, L. J.; Goto, Y.; Kurotso, T.; Palleros, D. R. Classification of Acid Denaturation of Proteins: Intermediates and unfolded states. *Biochemistry* **1994**, 33, 12504-12511.
(97) Maxwell, K. L.; Wildes, D.; Zarrine-Afsar, A.; De Los Rios, M. A.; Brown, A. G.; Friel, C. T.; Hedberg, L.; Horng, J.-C.; Bona, D.; Miller, E. J.; Vallée-Bélisle, A.; Main, E. R. G.; Bemporad, F., et al. Protein folding: Defining a "standard" set of experimental conditions and a preliminary kinetic data set of two-state proteins. *Protein Sci.* **2005**, 14, 602-616.
(98) Abzalimov, R. R.; Bobst, C. E.; Salinas, P. A.; Savickas, P.; Thomas, J. J.; Kaltashov, I. A. Studies of pH-Dependent Self-Association of a Recombinant Form of Arylsulfatase A with Electrospray Ionization Mass Spectrometry and Size-Exclusion Chromatography. *Anal. Chem.* **2013**, 85, 1591-1596.
(99) Li, G. Y.; Huang, J. F.; Zheng, Z.; Cao, Q. J. W.; Tian, Y. W.; Huang, G. M.; Li, L. J.; Ruotolo, B. T. Bicarbonate buffers can promote crosslinking and alternative gas-phase dissociation pathways for multiprotein complexes. *Int. J. Mass Spectrom.* **2021**, 469, 10.
(100) Hedges, J. B.; Vahidi, S.; Yue, X.; Konermann, L. Effects of Ammonium Bicarbonate on the Electrospray Mass Spectra of Proteins: Evidence for Bubble-Induced Unfolding. *Anal. Chem.* **2013**, 85, 6469-6476.

For TOC Only

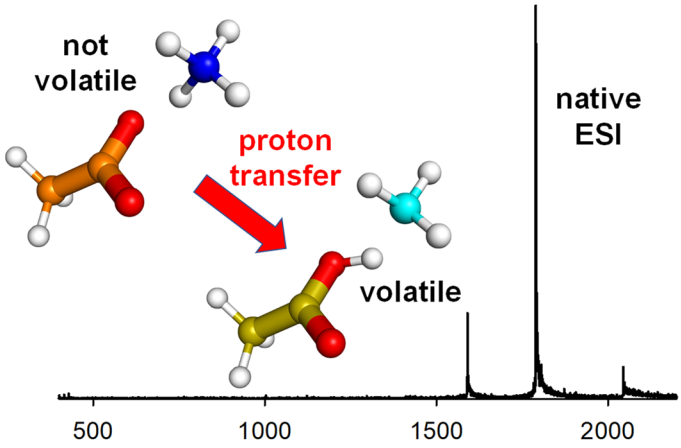
not
volatile
proton
transfer
volatile
native
ESI
500
1000
1500
2000